Bessel Beams for 6G - A Performance Analysis

Arjun Singh*, Innem V.A.K. Reddy†, Duschia Bodet‡ and Josep M. Jornet‡

*Department of Engineering
SUNY Polytechnic Institute, Utica, NY, USA E-mail: singha8@sunypoly.edu

†Department of Electrical Engineering
University at Buffalo SUNY, Buffalo, NY, USA E-mail: innemven@buffalo.edu

‡Department of Electrical and Computer Engineering
Northeastern University, Boston, MA, USA E-mail: {bodet.d, jmjornet}@northeastern.edu

2022 56th Asilomar Conference on Signals, Systems, and Computers | 978-1-6654-5906-8/22/$31.00 ©2022 IEEE | DOI: 10.1109/IEEECONF56349.2022.10052090

***Abstract*—The sixth-generation (6G) of wireless communications is expected to utilize (sub) terahertz (THz) frequencies in fulfilling the ambitious goals of very high data rates, ultra-low latency, and high density of interconnected devices. To combat the very high path losses at these frequencies, large antenna array apertures are required. However, due to the very large far-field distance of these arrays, the conventional assumptions of beamforming are compromised in most limits of wireless communications. Thus, it is necessary to engineer new wavefronts that are valid in the near field. This paper presents early results which indicate that Bessel beams, with a well-defined, non-diffracting propagating wavefront in the near-field, have promising applications in the next generation of wireless standards. Numerical results and their interpretations are provided to highlight that Bessel beams can perform better in near-field communication scenarios than canonical spherical and plane wave models. In addition, experimental results of a communication link at THz frequencies with Bessel beams are presented to further validate these as a contender for the "ideal" wavefront in 6G wireless standards.**

***Index Terms*—Terahertz communications; 6G; Bessel beams; Axicon;**

I. Introduction

The development of the sixth generation (6G) of wireless standards endeavors to reach tremendous milestones compared to the preceding wireless generations [1]–[3]. One nearly unanimously accepted goal for 6G standards is the ability to support wireless data rates reaching up to the 1 terabit-per-second (Tbps) mark. To sustain such data rates, new spectral resources are required to complement the microwave and millimeter (mmWave) bands that have been utilized in the fifth generation (5G) standards. While the free space optical (FSO) bands, operating in the infrared regime, provide a nearly boundless bandwidth [4], the very high path losses, health and safety concerns, and lack of dexterous and small devices make their utilization in ubiquitous wireless standards unfeasible [5].

In between the mmWave and FSO bands lies the terahertz (THz) band, defined as 0.1-10 THz [6]. The THz band provides a much larger bandwidth than the mmWave and microwave bands, without the safety concerns or the very high path losses of the FSO bands. THz-band communications have been investigated as one of the most promising breakthrough technologies for enabling the next generation of wireless standards [7], and several breakthrough developments in device technology have begun closing the so-called THz technology gap [8].

Nonetheless, the limited output power of small on-chip sources, the high path losses (as compared to the RF bands), and the susceptibility of THz communications to blockage still present pressing challenges in developing THz-band communications. The path loss includes the absorption loss and the spreading loss. The frequency selective absorption loss divides the THz-band into multi-GHz wide transmission windows. Thus its effect can be neglected if systems operate in a frequency band that avoids the absorption lines, many of which can still provide several GHz of contiguous bandwidth [9]. The spreading loss is proportional to the size of the antenna. As the high frequencies of the THz band constitute small (sub-millimeter) wavelengths, the size of the antennas and the corresponding received power density for typical antenna designs decreases [10]. This loss is further aggravated when therer is low transmit power, as is often the case with most THz communication systems [11].

Many envision using antenna arrays to generate high-gain, directional beams for THz-links to compensate for this high path loss [12]. In antenna arrays, multiple radiating elements are utilized to create an EM superposition that can concentrate the energy into a narrow beam [10]. The narrower the beam, the larger the gain, or directivity, of the array. Owing to the very small wavelengths of THz frequencies, antenna arrays of many elements can still have a small physical size. For example, at 1 THz, a 10 cm planar array would provide a gain of 55 dB. Furthermore, the deployment of extremely large (few meters) intelligent reflecting surfaces (IRSs) is also expected to help sustain smart and efficient non-line-of-sight (NLoS) links, reducing the blockage problem [13]. Indeed, many works have shown that with high gains from many-element (yet physically small) arrays, multi-meter-long THz links are feasible, supporting high-rate, reliable transmission.

However, such studies are often conducted under two major assumptions: a) far-field operation of the array, and b) narrow-band communications. These assumptions are challenged at THz frequencies.More specifically, far-field operation cannot be considered valid for most scenarios unless the electrical

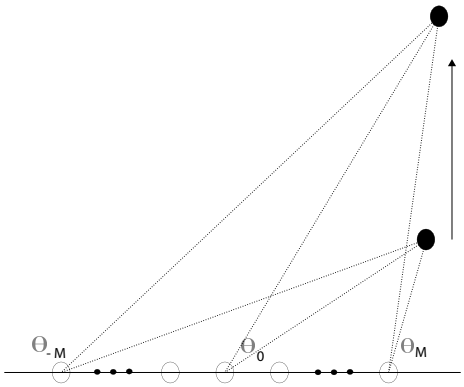

Fig. 1: The far-field assumption assumes that the angle of the point of interest from every element of the array is equal. Thus, $\theta_{-M} \approx \theta_M \approx \theta_0$, where θ_0 is the orientation from the centre of the array. Then, the corresponding path lengths, and subsequent phase delays, are thus linear values dependent on the central angle θ_0. In the far-field region, the maximum phase discrepancy from this simplification is $\pi/8$ and the assumption is considered valid

size and, therefore, the gain of the array is extremely limited. Thus high-gain THz arrays will often operate in the near field, where wavefront propagation is spherical [10] and traditional beamforming is no longer ideal. While near-field signal processing is being investigated both through beam focusing and customized radiation patterns using metasurfaces [14], [15], the question remains: does the manifestation of near-field communications in the (sub-)THz band necessarily constitute a problem, or can we, through an EM perspective, exploit radiation mechanisms to our benefit?

In this paper, we present Bessel beams as a promising solution for near-field THz band communications. First, in Sec. II, we revisit the near-field phenomenon and its likelihood in THz communications as a result of the link budget requirements. We expand upon the different radiating regimes and operation of an array in Sec. III. We also explain a simple method of generating Bessel beams which allows us to experimentally validate their exciting properties. We present our results in Sec. IV and conclude our paper in Sec. V.

II. Physics of Near-field Propagation

In this section, we explain the superposition principle that governs radiation from a large aperture and the corresponding near and far-field that are generated. We go on to explain why the near-field is so large in high-data-rate THz communications.

A. The Superposition Principle

An array acts as a large aperture device, in which each of the radiating elements radiates an EM signal. The superposition of these signals then describes the amplitude of the EM signal as generated by an array aperture. For an array in the x/y plane, centered at $Z = 0$, the resultant EM signal is given as [16]:

$$A(x,y,z) = \frac{1}{j\lambda}\iint_V A(\xi,\eta,0)\frac{\exp(-jkr_1)(1+cos\psi)}{2r_1}d\xi\, d\eta, \quad (1)$$

where the size of the array is $x = \xi; y = \eta$. The wave vector r_1 specifies the position vector, or propagation of the EM signal, from the origin $(0,0,0)$, and the angle ψ captures the deviation of the position vector from the transverse Z-axis. We notice that the complex amplitude $A(x,y,z)$ is related to the complex amplitude $A(\xi,\eta,0)$, or that the entire propagation is governed by the relation between the currents on the radiating elements. For a given distribution of sources across the array aperture, the individual EM signals add constructively at a position vector r_1 if the time delay, δt, between the path lengths of the EM signals is an integer multiple of the period of the signal. Thus, the time delay can be approximated as a phase delay $\delta\phi = 2\pi f \delta t$, where f is the signal frequency.

B. The Near-field Region

It is clear from the above discussion that every phase delay for a source on the array must be calculated as a relative phase delay compared to a central, or reference source. As an example in Fig. 1, the array has $2M+1$ elements, and the relative phases are all decided per the central element located at the origin. Then, based on the orientation of the position vector of the reference receiving point, every element has an individual path length that must be calculated and transformed into a subsequent phase delay for coherent superposition of the radiation.

However, as highlighted in Fig. 1, we notice that as the reference point is moved farther away from the array, the discrepancy in the angles decreases. Indeed, if the reference point is infinitely far away from the array, we can consider the same angle connecting the reference point with each element of the array. We thus define the far-field region as the distance beyond which we can safely assume the reference point to be far enough away from the array such that there are no severe discrepancies in the assumed and actual path lengths. In this case, the phase delays can be derived by assuming the same angle from the broadside across all the array elements. Indeed, the maximum discrepancy in these phase delays is then limited to $\pi/8$ [10], and array processing is significantly simplified by assuming the plane wave model.

For an array of side length D_1, operating at a design wavelength of λ, the boundary of the far-field D_{ff} is then given by by [10]:

$$D_{ff} \geq \frac{2D_1^2}{\lambda}. \quad (2)$$

If the receiving device is also an array, with a side length of D_2 such as in a multiple-input, multiple-output (MIMO) system, the far-field boundary is extended to:

$$D_{ff} \geq \frac{2(D_1+D_2)^2}{\lambda}. \quad (3)$$

It is worth noting that the boundary is thus dependent only on the electrical aperture and not the actual size of the device. When the link distance is less than the far-field boundary, the fundamental regime of operation is the near-field. Within the near-field, the radiating characteristics become more complex.

C. The Massive Near-field Region of THz Communications

For THz communications, devices will often be operating in this near-field region due to the high-gain, and therefore large antenna aperture dimensions, required by the path loss. We recall that a high signal-to-noise ratio (SNR) is desirable for low bit error rate (BER) and high data rate communications [17]. For reliable communications, the BER must be kept below a certain threshold. This BER threshold will corespond to a certain energy per bit, E_b, to the noise spectral density N_0, or E_b/N_0 threshold. Thus, for a given channel bit-rate f_b and a bandwidth B, the SNR must satisfy [17]:

$$SNR \geq 10\log_{10}\left(\frac{E_b}{N_0}\frac{f_b}{B}\right) + NF, \tag{4}$$

where NF accounts for the noise factor during demodulation prior to processing.

To achieve this desired SNR, the received power P_{RX} must satisfy

$$P_{RX} \geq SNR_{min} + N_0 B. \tag{5}$$

However, for a given transmitter power P_{TX}, the received power is determined by:

$$P_{RX} = P_{TX} - PL + G_{sys}, \tag{6}$$

where PL is the distance-dependent path loss, and G_{sys} is the combined gain of the system from the transmitter, receiver and (if present) any IRSs. The path loss over the link distance R from the Tx-Rx channel consists of the spreading loss and the absorption loss, and if an absorption-free transmission window is chosen, then the spreading loss dominates,

$$PL \approx 10\log_{10}\left(\frac{(4\pi R)^2}{\lambda^2}\right), \tag{7}$$

and increases as the wavelength decreases.

Thus, for higher spreading loss, we require a higher system gain. The gain G of a device is the effective measure of how concentrated the radiated power is in a given direction. The solid radiation angle Ω, of a device with linear (not dB) gain G_l is found as [10]:

$$\Omega = \frac{\pi^2}{G_l}, \tag{8}$$

assuming the directivity and gain to be equal. At the same time, we observe that for a square, planar array with a side length L, we have [10]:

$$\Omega = \left(\frac{\lambda}{2\pi}\right)^2 \left(\frac{2.782}{L}\right)^2, \tag{9}$$

and thus, we need a minimum side length to guarantee the desired gain. Therefore, for the required gain G_l, the side length L must satisfy:

$$L \geq \left(\frac{\lambda}{2\pi^2}\right)\left(2.782\sqrt{G_l}\right). \tag{10}$$

Thus, using (2) we see that the far-field distance of this device would be [10]:

$$D_{ff} = 2\frac{L^2}{\lambda} = \frac{\lambda}{2\pi^4} 2.782^2 G_l, \tag{11}$$

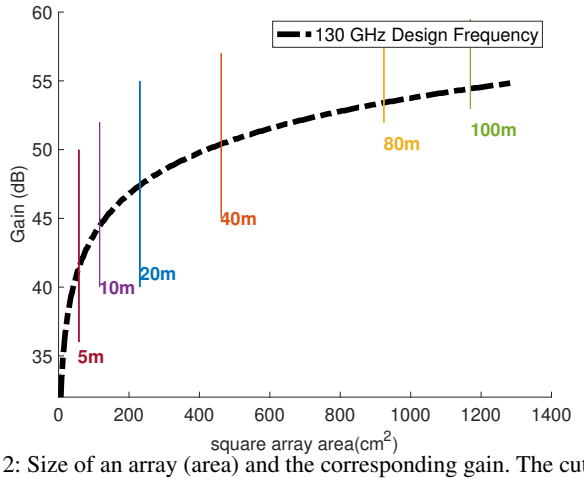

Fig. 2: Size of an array (area) and the corresponding gain. The cutouts indicate the far-field values at these sizes. Designs are at 130 GHz carrier.

where, once again, the gain is a linear expression. Thus, we notice that as the required absorption loss increases, the required gain and thus the corresponding near-field zone increases substantially.

We present the relation between the gain and near-field distance in Fig. 2. We observe that the large size of the planar, square array that satisfies the gain requirement also increases the corresponding far-field distance, which is presented at certain key values. Furthermore, as the gain is a non-linear relation to the area of the device, we need a substantial increase in the size, and therefore the far-field distance, to continue to provide for a larger gain.

III. Possible Near-field Solutions

In this section, we discuss some of the fundamental beam shapes that can be generated by an array and the corresponding required wavefronts.

A. Beamforming vs. Beam Focusing

In the far-field, beamforming is often the preferred method of achieving high power gains from antenna arrays. Here, the electric field from (1) is expressed towards a direction specified through spherical coordinates (θ, ϕ). The required phases, as described in Sec. II-A, are then found and applied to the array elements in the form of a codebook across the array $C(\Phi)$ given by [10]:

$$C(\Phi) = -k(d\sin\theta(\Delta x\cos\phi + \Delta y\sin\phi)), \tag{12}$$

with d as the separation between the elements. An increase in Δx or Δy signifies the particular element of the array that the codebook is applicable to.

As shown in Fig. 3(a), when the aperture is large, beamforming plane wave approximation results in the beam not yet being "formed" for quite some distance. Thus in order to achieve a high gain in the region close to the array (i.e. in the near field), the codebook must be calculated considering the precise location coordinates of each antenna element and the receiving point. This approach is known as *beam focusing*,

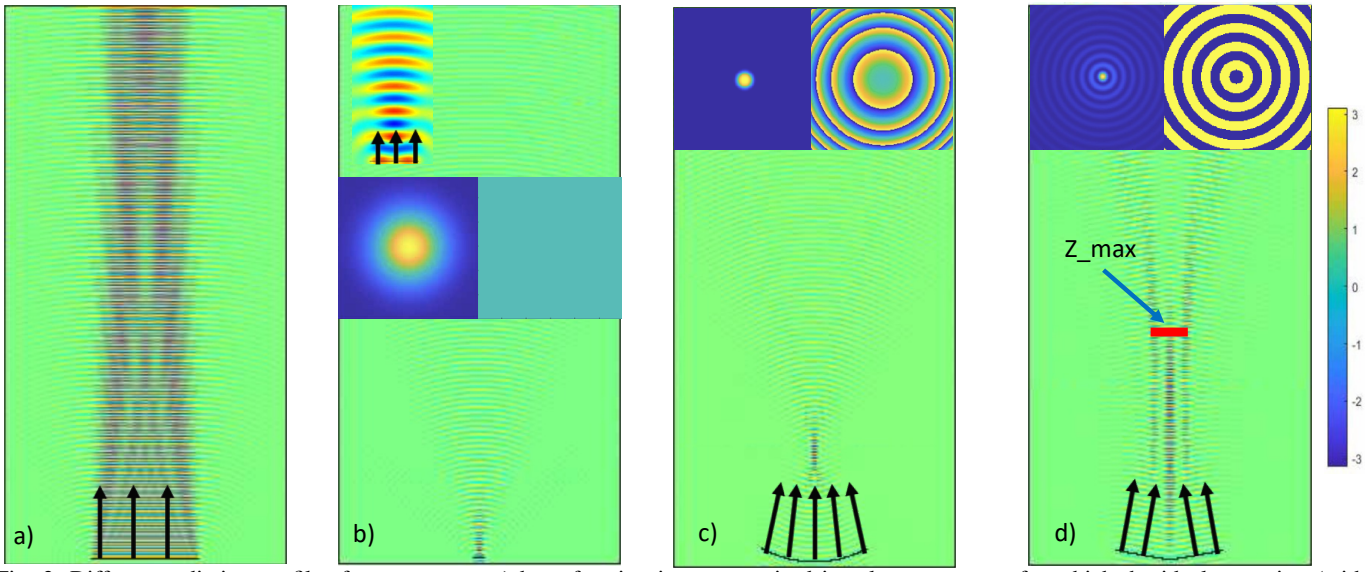

Fig. 3: Different radiation profiles from an array: a) beamforming is compromised in a large aperture, for which the ideal operation (with a smaller aperture) is shown in b), with the inset providing a zoomed perspective on the radiation; c) beamfocusing; and d) Bessel beams. The side by side insets in b), c), d) showcase the beam intensity and phase profile respectively. Black arrows indicate wavefront direction and the color bar indicates phase in radians.

and in this case, we must use a quadratic phase which captures the phase from a spherical wave generated by the transmitter array within the near-field, as shown in Fig. 3(c). The result is the beam focusing at a particular spot in space rather than in a given direction. The required codebook $C(\phi)$ is then:

$$C(\Phi) = e^{+jkr_1}, \tag{13}$$

providing an exact conjugate of the individual path distance from each element to the RX, with the convergence at a specific spot [10]. The resolution (beam-spot) F governed by the Abbe limit [18], which in an aperture of size R is:

$$F = 1.02\lambda/(R/2). \tag{14}$$

We observe that beam focusing is equivalent to beamforming if we assume the focusing point to be at infinity - effectively, beyond the near-field and in the far-field, the focused beam spot is equivalent to a beamwidth, and the plane wave approximation is sufficient for determining the phases required.

Clearly, beam focusing requires precise location coordinates, and thus the demands on channel estimation are quite high, even for micro-mobility scenarios. These requirements lead us to explore an alternative solution.

B. Bessel Beams in the Near-field

With the likelihood of a massive near-field in THz communications and the fact that the simplest spherical model comes with inbuilt limitations on location and propagation, we identify other beam shapes that are possible in the near-field. Notably, Bessel beams, first introduced by Durnin *et. al* in [19], possess a beam profile $B(x, y, z)$ given as:

$$B(x, y, z) = J_l(k_r\sqrt{x^2 + y^2})exp(jk_z z)exp(jl\tan^{-1}(y/x)), \tag{15}$$

where the wavevector k has the radial and transverse components k_r and k_z respectively, satisfying $k_z^2 + k_r^2 = k^2$. $J_l(\cdot)$ is the l-order Bessel function, and the intensity of such a beam remains independent of the distance of propagation. Thus, within the propagation distance of the Bessel beam in the near-field, the beam does not experience spreading losses. The characteristic beam profile is seen in Fig. 3(d), with the insets showing the non-diffracting beam intensity. The wavefront of such beams is similar to plane waves traveling inwards on a cone; for a cone angle θ, the codebook that satisfies a Bessel beam generation is given as:

$$C(\Phi) = k\sqrt{x^2 + y^2}sin(\theta). \tag{16}$$

The zero-order Bessel with $l = 0$ has a bright central spot, with multiple concentric rings around it, which are all in phase. Thus, the power transmitted to a receiver depends on the number of concentric rings that can be captured by it. The relation between the central spot size is determined by the zeros of the Bessel function, which thus depends on the radial wavevector k_r.

While true Bessel beams, which maintain a diffraction-free profile regardless of the propagation distance, require infinite power [19] a finite aperture produces a finite distance quasi-Bessel beam. As shown in Fig. 4(a), for a finite aperture of $2R$, the maximum distance of propagation Z_{max}, is found as [20]:

$$Z_{max} = \frac{R}{tan(\theta)}, \tag{17}$$

in which θ is the cone angle.

C. Generation of a Bessel Beam through an Axicon

As shown in Fig. 4(a), a Bessel beam can be generated through an array, with the phase difference given by

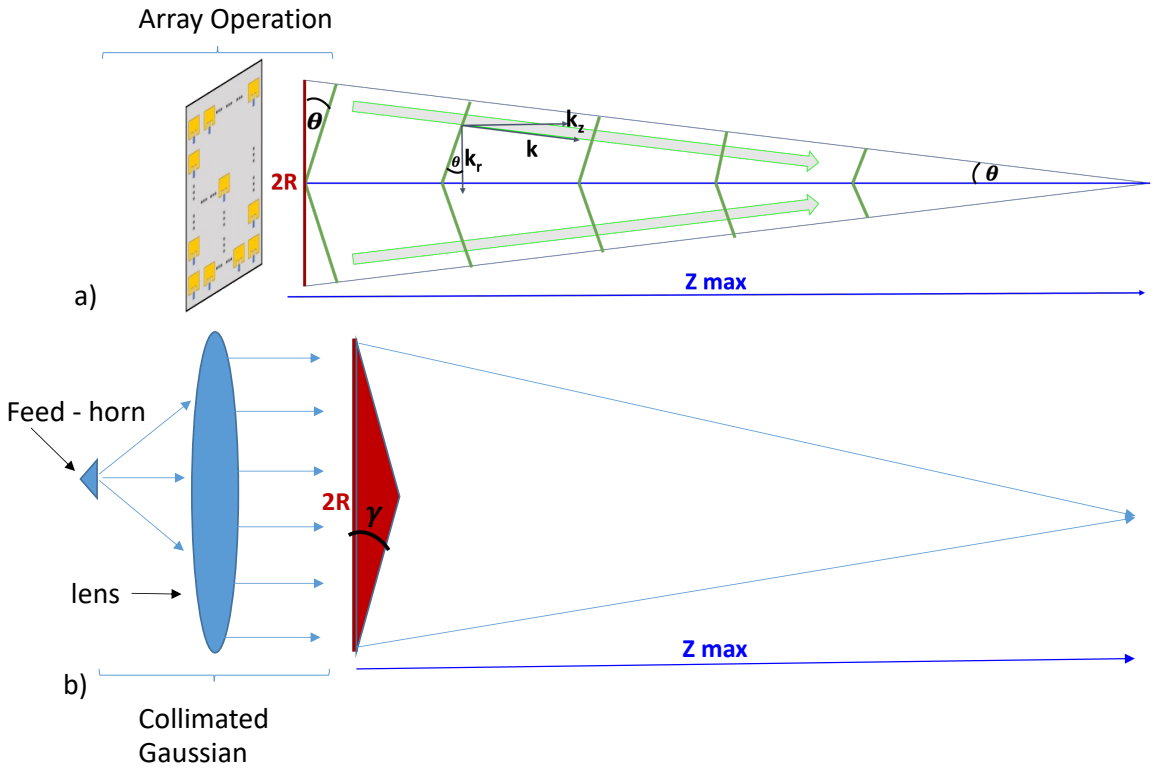

Fig. 4: Bessel Beam Generation: a) An Array that creates a Bessel with a cone angle θ can be mimicked by; b) an Axicon that receives a collimated Gaussian beam of the same aperture size. The Axicon angle γ must be matched to the relation of the cone angle and the refractive index η.

(16). At the same time, as shown in Fig. 4(b), the same is possible through a custom-designed lens, or axicon. This axicon has a pyramid-shaped thickness, which imparts the conical phase [21]. For an axicon with refractive index η, the equivalent relation between the axicon opening angle γ and the cone angle θ of the Bessel, is given as:

$$\theta = tan^{-1}\left((\eta - 1)\gamma\right), \tag{18}$$

assuming that the axicon and the array have the same aperture. The axicon must receive a planar Gaussian beam at the incident side. For this, the radiation from a horn antenna can be collimated through the utilization of a lens, i.e., the utilization of a horn-lens antenna.

IV. Experimental Validation

In this section, we present our results to indicate the efficiency and requirement of Bessel beams in (sub) THz communications for realizing 6G and beyond key performance indicators.

A. Experimental Set-up

Using the TeraNova testbed [22], we generate single-carrier information signals at an intermediate frequency (IF) in MATLAB with a variety of badnwidths and modualtion orders. These digital IF signals are converted to analog signals using a Keysight arbiitrary waveform generator. The result is upconverted to a carrier frequency of 130 GHz with a custom-designed front-end from Virginia Diodes (VDI). The signal

Fig. 5: Experimental Testbed in which the Axicon is mounted directly atop the horn-lens antenna, seen on the left.

then travels through a 40 dBi lens antenna that generates a collimated Gaussian beam, functioning as the front portion of the setup explained in Fig. 4(b). A 3-D printed axicon of the same size as the lens, 11.8 cm, is attached to the front of the lens to transform the information-bearing Gaussian beam into a Bessel beam. The axicon material is Polylactic acid (PLA), with a refractive index of approximately 1.6 at 130 GHz frequency, and very low material losses.

The receiver is placed 40 cm away from the transmitter and uses a 21 dBi antenna to capture the signal at the non-diffracting region of the Bessel beam. The signal is downconverted to an IF before a Keysight Digital Storage Oscilloscope

General	
Link Distance, h	40 cm
Transmitted power, P_{tx}	7.5 dBm
Transmitter antenna gain, G_{tx}	40 dBi
Receiver antenna gain, G_{rx}	21 dBi

TABLE I: System parameters

Bandwidth	Modulation Order	Bit Rate	Bessel BER
5 GHz	16	10 Gbps	<2.08e-4
5 GHz	64	15 Gbps	<1.3889e-4
5 GHz	256	20 Gbps	4.1667e-4
20 GHz	16	40 Gbps	<2.08e-4
20 GHz	64	60 Gbps	0.0131
20 GHz	256	80 Gbps	0.0833

TABLE II: Performance of Information-Bearing Bessel Beams at 130 GHz

(DSO) digitizes and stores the IF signal. The In-Phase and Quadrature (IQ) symbols as well as the originally transmitted bitstream are then retrieved.

B. Multi-Gbps Links with THz Bessel Beams

The achieved bit rates and BERs are shown in Table II, and the received IQ constellations are shown in Fig. 6(a-if, for different signal bandwidth and modulation order. For higher-order QAM modulations, the bit rate increases but the error probability also increases. Similarly, utilizing more bandwidth enables higher bit rates, but can lead to a higher error probability. Nonetheless, we see that Bessel beams can achieve 40 Gbps with 20 GHz of bandwidth and a 16-QAM modulation scheme in single-carrier near-field sub-THz communications.

V. Conclusions

In this paper, we emphasized the importance of correctly determining the radiating regime of devices that can be expected to provide high data rate communications in the next generation of wireless standards. With the likelihood of the near-field, the conventional plane wave model becomes invalid, and the spherical wave model is inefficient. Exploiting other near-field designs, such as Bessel beam-generating conical wavefronts, can provide robust communication links. We highlighted how Bessel beams can be generated both through arrays as well as lens-like Axicons. Our results highlight both the massive near-field region of (sub) THz-communications, as well as the first multi-Gbps link at these frequencies through Bessel beams.

References

[1] I. F. Akyildiz *et al.*, "Terahertz band communication: An old problem revisited and research directions for the next decade," *IEEE Trans. on Commun.*, vol. 70, no. 6, pp. 4250–4285, June 2022.

[2] I. F. Akyildiz, A. Kak, and S. Nie, "6g and beyond: The future of wireless communications systems," *IEEE Access*, vol. 8, pp. 133 995–134 030, 2020.

[3] ATISn, "NextG Alliance," 2021, accessed: December 10, 2019.

[4] E. Ciaramella, Y. Arimoto, G. Contestabile, M. Presi, A. D'Errico, V. Guarino, and M. Matsumoto, "1.28 terabit/s (32x40 gbit/s) wdm transmission system for free space optical communications," *IEEE Journal on selected areas in communications*, vol. 27, no. 9, pp. 1639–1645, 2009.

[5] R. E. Miles, X.-C. Zhang, H. Eisele, and A. Krotkus, *Terahertz frequency detection and identification of materials and objects*. Springer Science & Business Media, 2007.

[6] I. F. Akyildiz, J. M. Jornet, and C. Han, "Terahertz band: Next frontier for wireless communications," *Physical Communication*, vol. 12, pp. 16–32, 2014.

[7] T. S. Rappaport, Y. Xing, O. Kanhere, S. Ju, A. Madanayake, S. Mandal, A. Alkhateeb, and G. C. Trichopoulos, "Wireless communications and applications above 100 GHz: Opportunities and challenges for 6G and beyond," *IEEE Access*, vol. 7, pp. 78 729–78 757, 2019.

[8] K. Sengupta, T. Nagatsuma, and D. M. Mittleman, "Terahertz integrated electronic and hybrid electronic–photonic systems," *Nature Electronics*, vol. 1, no. 12, p. 622, 2018.

[9] J. M. Jornet and I. F. Akyildiz, "Channel modeling and capacity analysis for electromagnetic wireless nanonetworks in the terahertz band," *IEEE Transactions on Wireless Communications*, vol. 10, no. 10, pp. 3211–3221, 2011.

[10] C. A. Balanis, *Antenna theory: analysis and design*. John Wiley & Sons, 2016.

[11] J. V. Siles, K. B. Cooper, C. Lee, R. H. Lin, G. Chattopadhyay, and I. Mehdi, "A new generation of room-temperature frequency-multiplied sources with up to 10× higher output power in the 160-ghz–1.6-thz range," *IEEE Transactions on Terahertz Science and Technology*, vol. 8, no. 6, pp. 596–604, 2018.

[12] I. F. Akyildiz and J. M. Jornet, "Realizing ultra-massive MIMO (1024×1024) communication in the (0.06–10) terahertz band," *Nano Communication Networks*, vol. 8, pp. 46–54, 2016, U.S. Patent No. 9,825,712, November 21, 2017 (Priority Date: Dec. 6, 2013).

[13] M. Di Renzo, M. Debbah, D.-T. Phan-Huy, A. Zappone, M.-S. Alouini, C. Yuen, V. Sciancalepore, G. C. Alexandropoulos, J. Hoydis, H. Gacanin *et al.*, "Smart radio environments empowered by reconfigurable ai meta-surfaces: An idea whose time has come," *EURASIP Journal on Wireless Communications and Networking*, vol. 2019, no. 1, pp. 1–20, 2019.

[14] C. Liaskos, S. Nie, A. Tsioliaridou, A. Pitsillides, S. Ioannidis, and I. Akyildiz, "A novel communication paradigm for high capacity and security via programmable indoor wireless environments in next generation wireless systems," *Ad Hoc Networks*, vol. 87, pp. 1–16, 2019.

[15] K. Dovelos, S. D. Assimonis, H. Q. Ngo, B. Bellalta, and M. Matthaiou, "Intelligent reflecting surfaces at terahertz bands: Channel modeling and analysis," *arXiv preprint arXiv:2103.15239*, 2021.

[16] F. Depasse, M. Paesler, D. Courjon, and J. Vigoureux, "Huygens–fresnel principle in the near field," *Optics letters*, vol. 20, no. 3, pp. 234–236, 1995.

[17] A. Goldsmith, *Wireless communications*. Cambridge university press, 2005.

[18] E. Abbe, "Contributions to the theory of the microscope and microscopic perception," *Archive for microscopic anatomy*, vol. 9, no. 1, pp. 413–468, 1873.

[19] J. Durnin, "Exact solutions for nondiffracting beams. I. the scalar theory," *JOSA A*, vol. 4, no. 4, pp. 651–654, 1987.

[20] J. Durnin, J. Miceli, and J. H. Eberly, "Comparison of bessel and gaussian beams," *Optics letters*, vol. 13, no. 2, pp. 79–80, 1988.

[21] J. Arlt and K. Dholakia, "Generation of high-order bessel beams by use of an axicon," *Optics Communications*, vol. 177, no. 1-6, pp. 297–301, 2000.

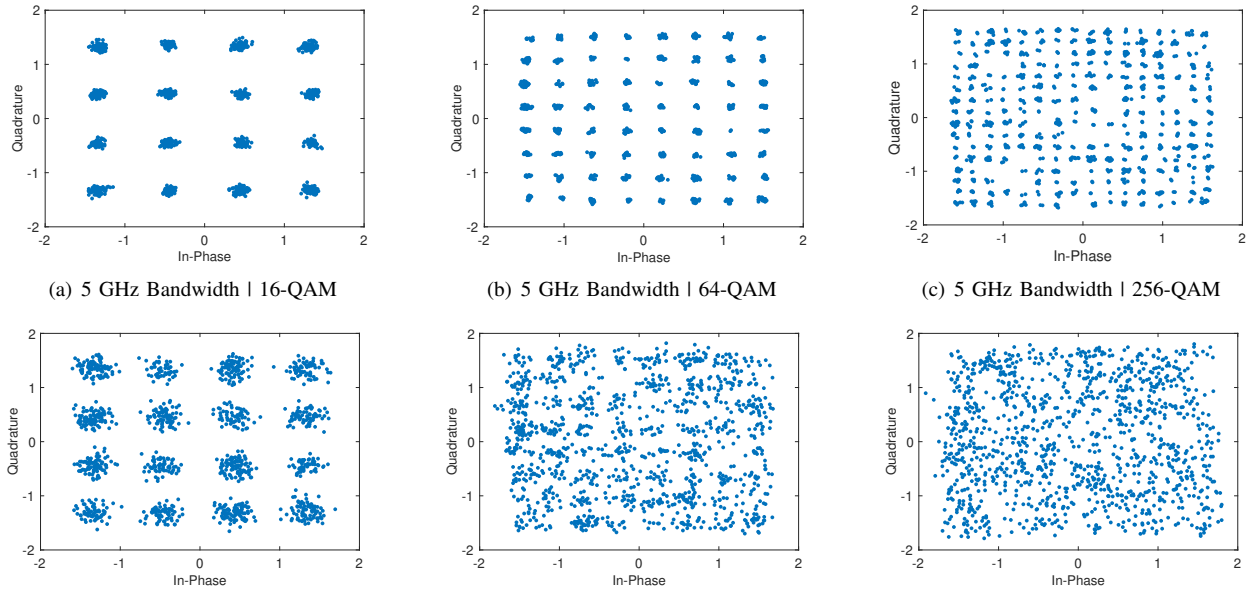

(a) 5 GHz Bandwidth | 16-QAM (b) 5 GHz Bandwidth | 64-QAM (c) 5 GHz Bandwidth | 256-QAM

(d) 20 GHz Bandwidth | 16-QAM (e) 20 GHz Bandwidth | 64-QAM (f) 20 GHz Bandwidth | 256-QAM

Fig. 6: Received IQ constellations of information-bearing bessel beams

[22] P. Sen, V. Ariyarathna, A. Madanayake, and J. M. Jornet, "Experimental wireless testbed for ultrabroadband terahertz networks," in *Proceedings of the 14th International Workshop on Wireless Network Testbeds, Experimental evaluation & Characterization*, 2020, pp. 48–55.